Supplementary Materials

The phase transition tuning by the Fe(III)/Co(III) substitution in switchable cyano-bridged perovskites: $[C_3N_2H_2]_2[KFe_XCo_{1-X}(CN)_6]$

Magdalena Rok[ab]†, Marcin Moskwa[a], Andrzej Pawlukojć[bc], Rafał Janicki[a], Iga Zuba[bc], Piotr Zieliński[d], Paweł Sobieszczyk[d], Grażyna Bator[a]

[a]Faculty of Chemistry, University of Wroclaw, F. Joliot–Curie 14, 50-383 Wrocław, Poland
[b]Frank Laboratory of Neutron Physics, Joint Institute for Nuclear Research, Joliot–Curie 6, 141-980 Dubna, Russia
[c]Institute of Nuclear Chemistry and Technology, Dorodna 16, 03-195 Warszawa, Poland
[d]The H. Niewodniczański Institute of Nuclear Physics PAS, Radzikowskiego 152, 31-342 Kraków, Poland
† e-mail: magdalena.rok@chem.uni.wroc.pl

CAPTIONS OF FIGURES

CAPTIONS OF TABLES

Table S1. Masses and number of moles of mixed crystals **IMFe$_x$Co$_{1-x}$**.

Theoretical X molar fraction of Fe^{3+}	$K_3Fe(CN)_6$		$K_3Co(CN)_6$		1H-Imidazole hydrochloride		Obtained X molar fraction of Fe^{3+}
	$m_{Fe^{3+}}$ [g]	$n_{Fe^{3+}}$ [mol]	$m_{Co^{3+}}$ [g]	$n_{Co^{3+}}$ [mol]	$m_{imid.HCl}$ [g]	$n_{imid.HCl}$ [mol]	
IMCo, 0	0.00	0.00	3.00	9.0E-03	2.83	2.7E-02	**IMCo**, 0
0.2	0.62	1.9E-03	2.50	7.5E-03	2.95	2.8E-02	0.29
0.3	0.85	2.6E-03	2.00	6.0E-03	2.70	2.6E-02	0.42
0.4	1.32	4.0E-03	2.00	6.0E-03	3.15	3.0E-02	0.51
0.5	1.49	4.5E-03	1.50	4.5E-03	2.83	2.7E-02	0.63
0.6	2.23	6.8E-03	1.50	4.5E-03	3.54	3.4E-02	0.70
0.8	3.17	9.6E-03	0.80	2.4E-03	3.77	3.6E-02	0.85
IMFe, 1	3.00	9.1E-03	0.00	0.0E+00	2.86	2.7E-02	**IMFe**, 1

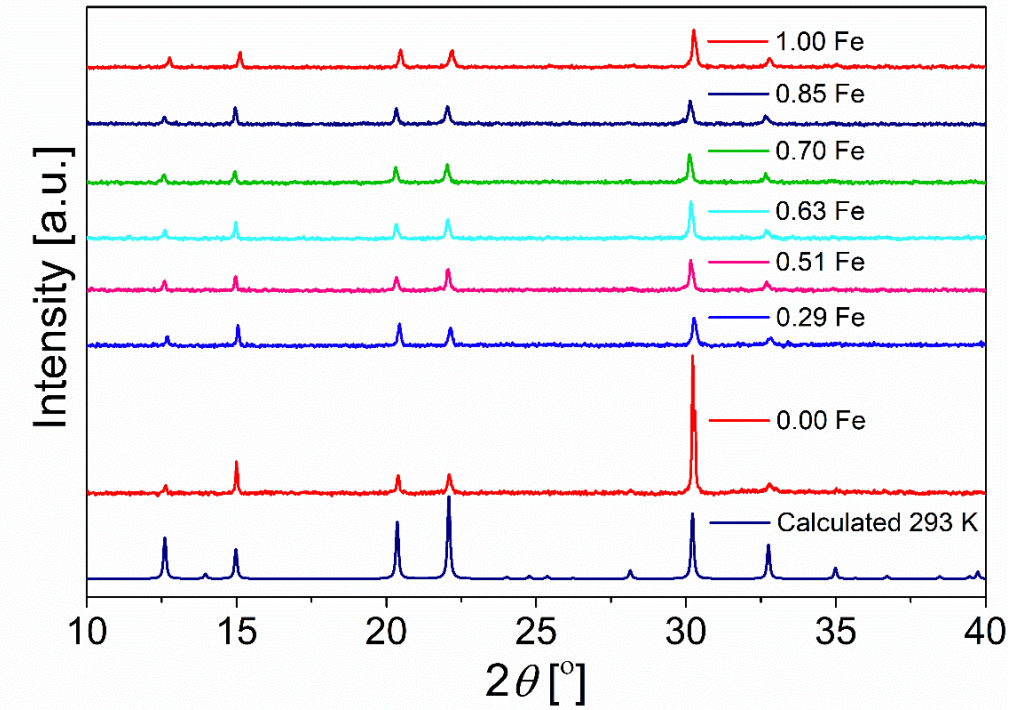

Fig. S1. X-ray diffraction pattern of **ImFe$_x$Co$_{1-x}$** (x: 0.00-1.00) at 298 K and calculated from crystal structure IMCo.

Table S2. Crystal data, experimental details, and structure refinement results for **IMFe$_{0.42}$Co$_{0.58}$** at 298, 170 and 100 K.

	ImFeCo298K	**ImFeCo**170K	**ImFeCo**100K
Chemical formula		$(C_3H_5N_2)_2[KFe_{0.42}Co_{0.58}(CN)_6]$	
M_r		391.03	
Crystal system, space group	Trigonal, $R\bar{3}m$	Trigonal, $R\bar{3}$	Monoclinic, $A2/a$*
Temperature (K)	298(2)	170(2)	100(2)
a, b, c (Å)	8.747(3), 8.747(3), 19.074(3)	8.763(2), 8.763(2), 18.800(4)	15.089(2), 8.773(3), 13.454(2)
β (°)	90	90	111.74(3)
V (Å^3)	1264(2)	1250(2)	1654(3)
Z	3	3	4
Radiation type	Mo $K\alpha$	Mo $K\alpha$	Mo $K\alpha$
μ (mm^{-1})	1.23	1.24	1.25
Crystal size (mm)	0.39×0.30×0.16	0.39×0.30×0.16	0.39×0.30×0.16
Absorption correction	Analytical	Analytical	Analytical
T_{min}, T_{max}	0.760, 0.903	0.723, 0.874	0.736, 0.871
No. of measured, independent and observed [$I > 2\sigma(I)$] reflections	1850, 324, 310	4619, 526, 521	5343, 1546, 1366
R_{int}	0.071	0.081	0.065
$(\sin \theta/\lambda)_{max}$ (Å^{-1})	0.605	0.604	0.606
$R[F^2 > 2\sigma(F^2)]$, $wR(F^2)$, S	0.037, 0.098, 1.10	0.052, 0.135, 1.31	0.051, 0.141, 1.12
No. of reflections	324	526	1546
No. of parameters	29	41	111
$\Delta\rho_{max}/\Delta\rho_{min}$ [e A^{-3}]	0.30/-0.43	0.44/-0.63	0.57/-0.40

* - non-standard setting of $C2/c$ space group (no. 15)

Table S3. Atomic concentration (%) of mixed crystal obtained on EDS results.

$[C_3H_5N_2]_2[KFe_xCo_{1-x}(CN)_6]$						
X Fe^{3+}	**No.**	**C [%]**	**N [%]**	**K [%]**	**Fe [%]**	**Co [%]**
0.0	1	43.04	38.88	8.89	0.00	9.19
	2	43.60	37.53	9.33	0.00	9.54
	3	42.84	37.67	9.70	0.00	9.79
	4	42.63	38.23	9.55	0.00	9.59
	Average	**43.03**	**38.08**	**9.37**	**0.00**	**9.53**
0.29	1	38.88	44.43	8.25	2.37	6.08
	2	38.85	44.03	8.48	2.45	6.19
	3	39.2	44.03	8.34	2.51	5.92
	4	38.58	44.81	8.23	2.51	5.87
	Average	**38.88**	**44.33**	**8.33**	**2.46**	**6.02**
0.51	1	38.25	45.29	8.07	4.19	4.2
	2	37.65	45.07	8.51	4.41	4.36
	3	37.48	45.1	8.57	4.63	4.22
	4	37.49	45.63	8.27	4.51	4.1
	Average	**37.72**	**45.27**	**8.36**	**4.44**	**4.22**
0.63	1	36.14	44.86	9.24	6.35	3.41
	2	35.79	44.22	9.76	6.53	3.72
	3	35.59	44.57	9.75	5.98	4.11
	4	35.22	44.24	10.16	6.58	3.8
	Average	**35.69**	**44.47**	**9.73**	**6.36**	**3.76**
0.70	1	38.49	42.33	9.4	6.8	2.98
	2	37.02	44.34	9.14	6.52	2.98
	3	36.76	45.05	9.01	6.7	2.47
	4	38.01	44.1	8.75	6.41	2.74
	Average	**37.57**	**43.96**	**9.08**	**6.61**	**2.79**
0.85	1	37.26	45.81	8.35	7.16	1.41
	2	40.05	40.85	9.36	8.23	1.52
	3	37.72	44.38	8.75	7.74	1.42
	4	38.68	44.38	9.19	8.17	1.33
	Average	**38.43**	**43.86**	**8.91**	**7.83**	**1.42**
1.0	1	39.43	45.54	7.37	7.65	0.00
	2	39.04	45.81	7.50	7.65	0.00
	3	38.77	45.03	7.94	8.26	0.00
	4	39.79	45.21	7.84	8.16	0.00
	Average	**39.26**	**45.40**	**7.66**	**7.93**	**0.00**

$[C_3H_5N_2]_2[KFe_xCo_{1-x}(CN)_6]$

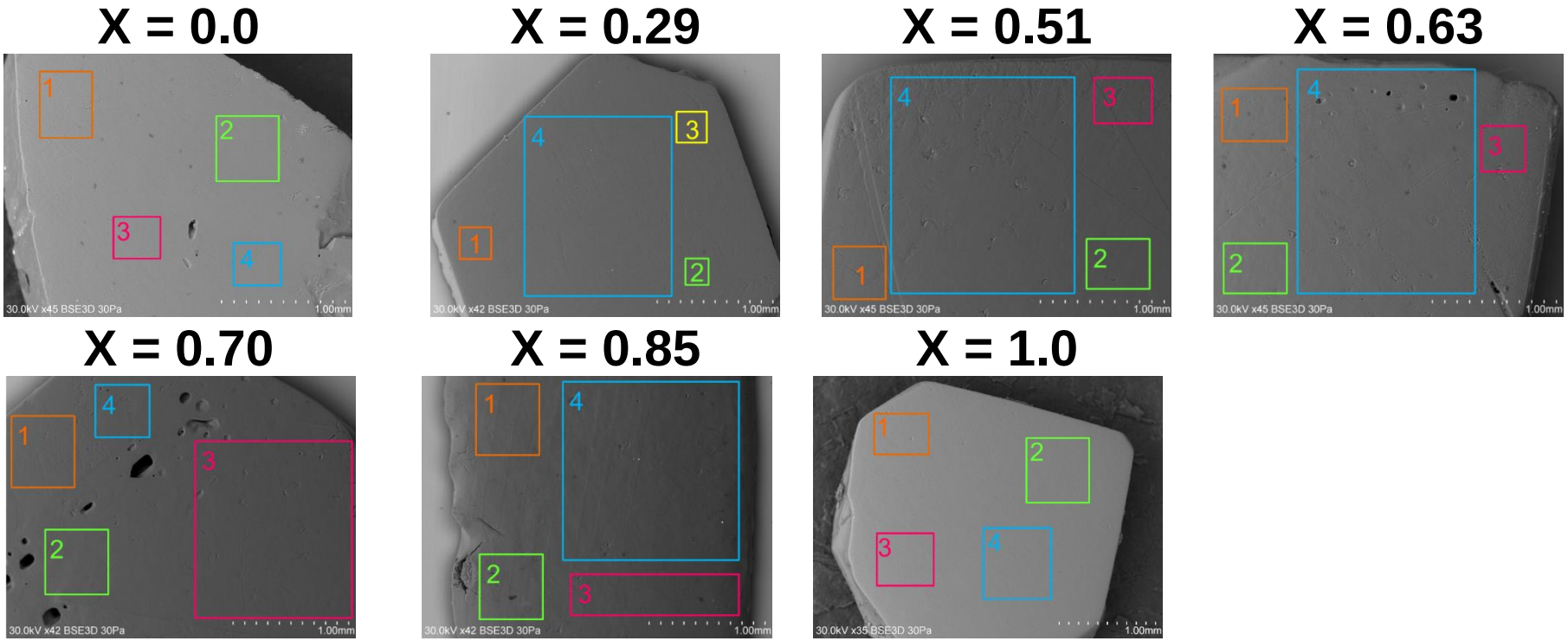

Fig. S2. SEM photographs of pure and mixed-crystals. Four squares represent the measured areas.

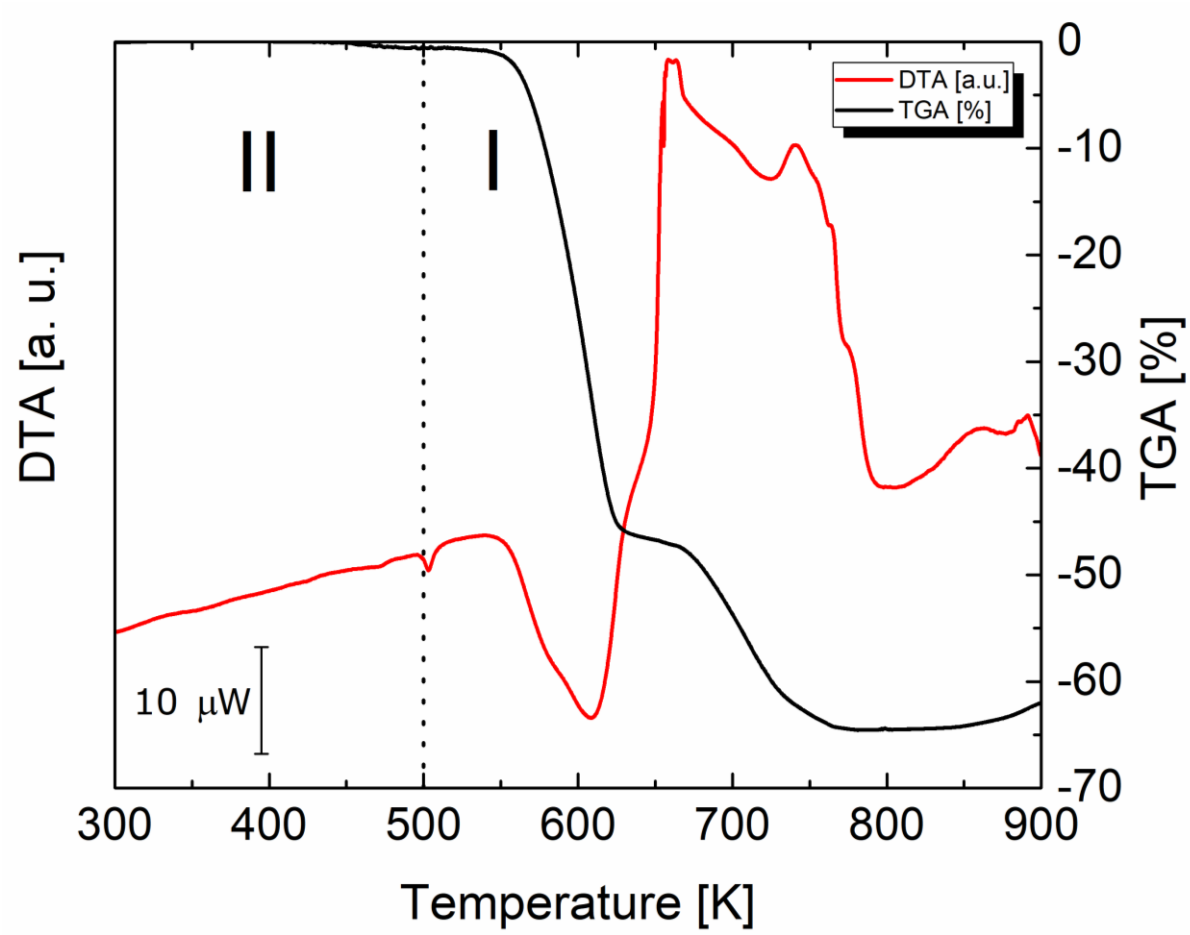

Fig. S3. TGA and DTA thermograms between 300 and 900 K measured for **IMCo**

Table S4. Thermodynamic parameters of phase transitions for **IMFe$_x$Co$_{1-x}$**, x = 0, 0.29, 0.51, 0.63, 0.7, 0.85, 1.0 in the condensed state.

PT	**IV → III**						
$X_{Fe^{3+}}$	**0.0**	**0.29**	**0.51**	**0.63**	**0.7**	**0.85**	**1.0**
M [g/mol]	392.4	391.5	390.8	390.4	390.2	389.7	389.3
T [K]	157.9	124.5	135.3	141.7	142.3	151.6	157.9
ΔH [J·g^{-1}]	7.63	6.08	7.11	7.28	7.05	7.97	7.63
ΔH [J·mol^{-1}]	2993.63	2380.06	2778.44	2842.18	2750.87	3106.16	2970.13
ΔS [J·mol^{-1}·K^{-1}]	18.96	19.12	20.54	20.06	19.34	20.49	18.81
N	3.13	3.16	3.44	3.34	3.20	3.43	3.10
PT	**II → I**						
$X_{Fe^{3+}}$	**0.0**	**0.29**	**0.51**	**0.63**	**0.7**	**0.85**	**1.0**
M [g/mol]	392.4	391.5	390.8				
T [K]	502.0	500.0	496.6				
ΔH [J·g^{-1}]	11.2	11.48	11.9				
ΔH [J·mol^{-1}]	4394.32	4493.92	4650.27				
ΔS [J·mol^{-1}·K^{-1}]	8.75	8.99	9.36				
N	1.69	1.72	1.76				

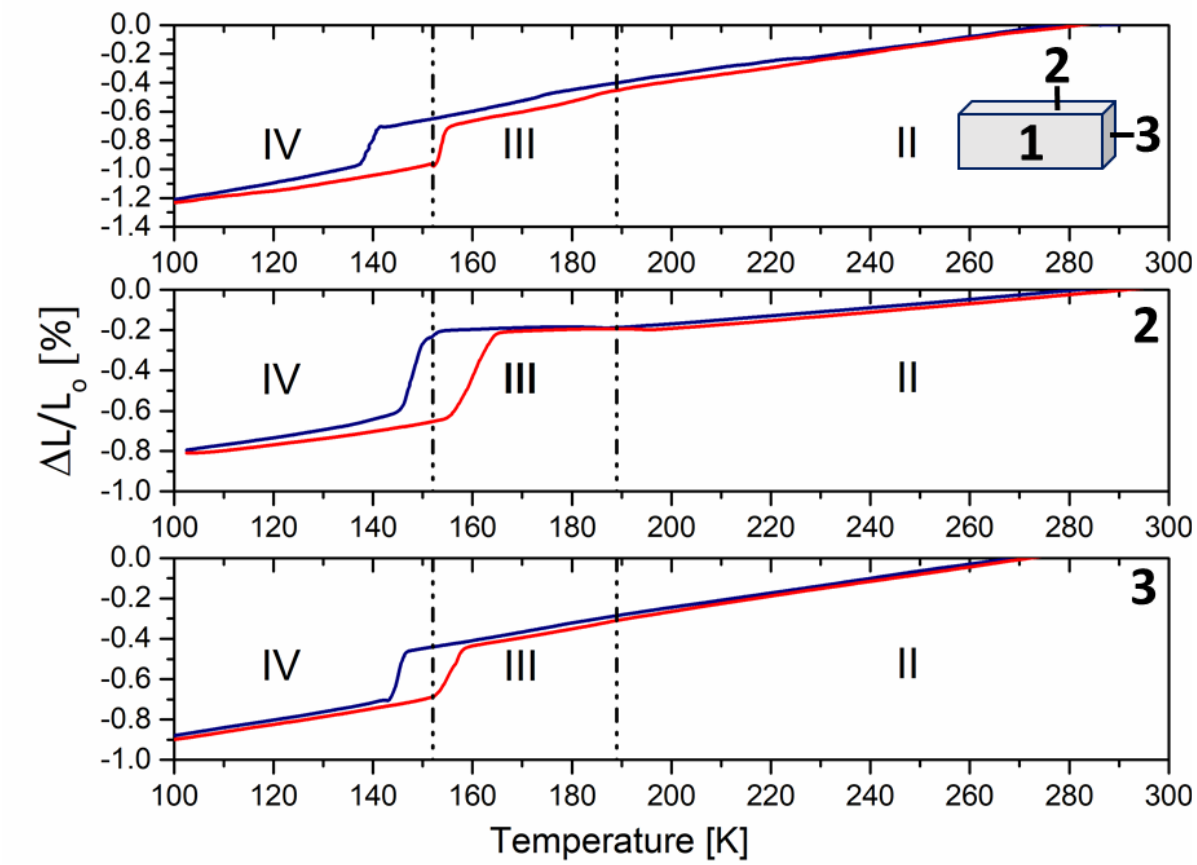

Fig. S4. Temperature dependences of relative changes of linear dimensions $\Delta L/L_o$ [%] curves for **IMFe$_x$Co$_{1-x}$,** x = 0.85 (temperature range from 100 to 280 K), measured along three perpendicular directions.

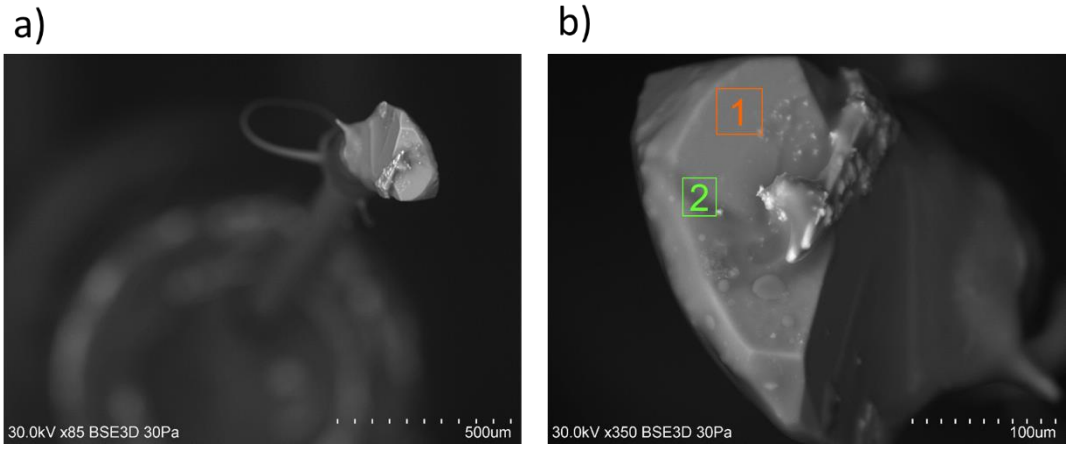

Fig. S5. SEM photographs of mixed crystal **IMFe$_{0.42}$Co$_{0.58}$** after X-ray measurement in IV, III, II phases. a) The picture of a fixed crystal on pin, b) two squares represent the measured EDS areas.

Table S5. Atomic concentration (%) of **IMFe$_{0.42}$Co$_{0.58}$** crystal obtained on EDS results.

X Fe^{3+}	No.	Fe [%]	Co [%]
0.42	1	41.26	58.74
	2	43.52	56.48
	Average	42.39	57.61

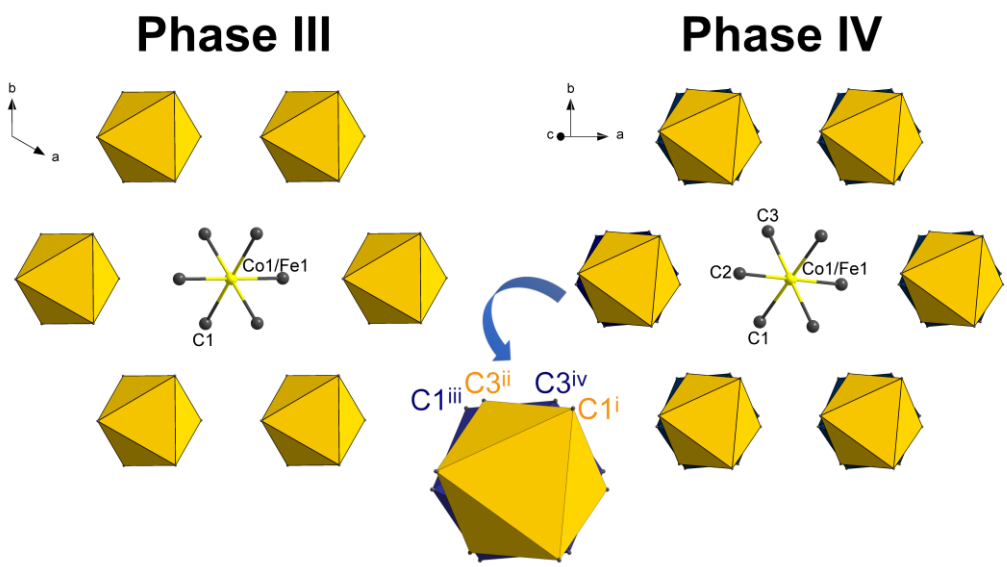

Fig. S6. In the Phase III, all hexacyanoferrate(III)/cobaltate(III) ions (presented as octahedron formed by Co/Fe and C atoms) are twisted in the same direction. In the Phase IV, by contrast, the octahedrons of hexacyanoferrate ions are twisted in opposite directions. Symmetry codes: (i) −x+2, −y+1/2, −z+5/2; (ii) x, y, z+1; (iii) −x+3/2, y, −z+1; (iv) x−1/2, −y+1/2, z−1/2.

Table S6. Hydrogen-bond geometry (Å, º) for **ImFe$_{0.42}$Co$_{0.58}$** at 100 K.

D*—H···*A	***D*—H**	**H···*A***	***D*···*A***	***D*—H···*A***
N1*A*—H1*A*···N1^{i}	0.88	2.60	3.217(4)	128
N1*A*—H1*A*···N2^{ii}	0.88	2.51	3.136(5)	129
N3*A*—H3*A*···N3^{ii}	0.88	2.11	2.980(4)	168

Symmetry codes: (i) −*x*+3/2, *y*, −*z*+1; (ii) *x*, *y*−1/2, *z*−1/2; (iii) −*x*+2, −*y*+1, −*z+1*.

Table S7. Selected bond lengths and the shortest M···K distances (Å) (where M: Fe(III)/Co(III), Fe(III), Co(III)) for **IMFe$_{0.42}$Co$_{0.58}$**, **IMFe**[1] and **IMCo**[2].

	M—C	K—N	C—N	M···K	M—C	K—N	C—N	M···K
	Phase II ($R\bar{3}m$)				Phase IV ($A2/a$)			
ImFe$_{0.42}$Co$_{0.58}$	1.922(2)	2.899(2)	1.148(3)	5.967(4)	1.929(4) 1.930(3) 1.934(3)	2.862(3) 2.875(3) 2.888(3)	1.157(4) 1.158(4) 1.159(4)	5.911(2) 5.938(2) 5.959(2)
ImFe[1]	1.940(2)	2.879(2)	1.148(3)	5.985(6)	1.949(4) 1.949(4) 1.950(4)	2.858(4) 2.864(4) 2.874(4)	1.148(5) 1.153(2) 1.155(2)	5.927(5) 5.934(5) 5.954(5)
ImCo[2]	1.901(2)	2.902(2)	1.146(3)	5.947(4)	1.902(4) 1.906(4) 1.908(4)	2.878(4) 2.887(4) 2.898(4)	1.148(5) 1.150(5) 1.152(5)	5.903(2) 5.923(2) 5.940(2)

Table S8. Cage volumes per unit cell (Å^3) for **ImFe$_{0.42}$Co$_{0.58}$**, **ImFe**[1,3] and **ImCo**[2]. The volume of a single cage calculated from the crystal structure with PLATON program[4]

	Phase II ($R\bar{3}m$)	Phase III ($R\bar{3}$)	Phase IV ($A2/a$)
ImFe$_{0.42}$Co$_{0.58}$	588.6	576.5	732.2
ImFe[1,3]	586.9	570.1	728.5
ImCo[2]	578.9	560.1	728.4

(1) Zhang, W.; Cai, Y.; Xiong, R.-G.; Yoshikawa, H.; Awaga, K. Exceptional Dielectric Phase Transitions in a Perovskite-Type Cage Compound. *Angew. Chemie Int. Ed.* **2010**, *49*, 6608–6610.

(2) Zhang, X.; Shao, X.-D.; Li, S.-C.; Cai, Y.; Yao, Y.-F.; Xiong, R.-G.; Zhang, W. Dynamics of a Caged Imidazolium Cation-toward Understanding the Order-Disorder Phase Transition and the Switchable Dielectric Constant. *Chem. Commun.* **2015**, *51*, 4568–4571.

(3) Phillips, A. E.; Fortes, A. D. Crossover between Tilt Families and Zero Area Thermal Expansion in Hybrid Prussian Blue Analogues. *Angew. Chemie - Int. Ed.* **2017**, *56* (50), 15950–15953.

(4) Van Der Sluis, P.; Spek, A. L. BYPASS: An Effective Method for the Refinement of Crystal Structures Containing Disordered Solvent Regions. *Acta Crystallogr. Sect. A* **1990**, *46*, 194–201.

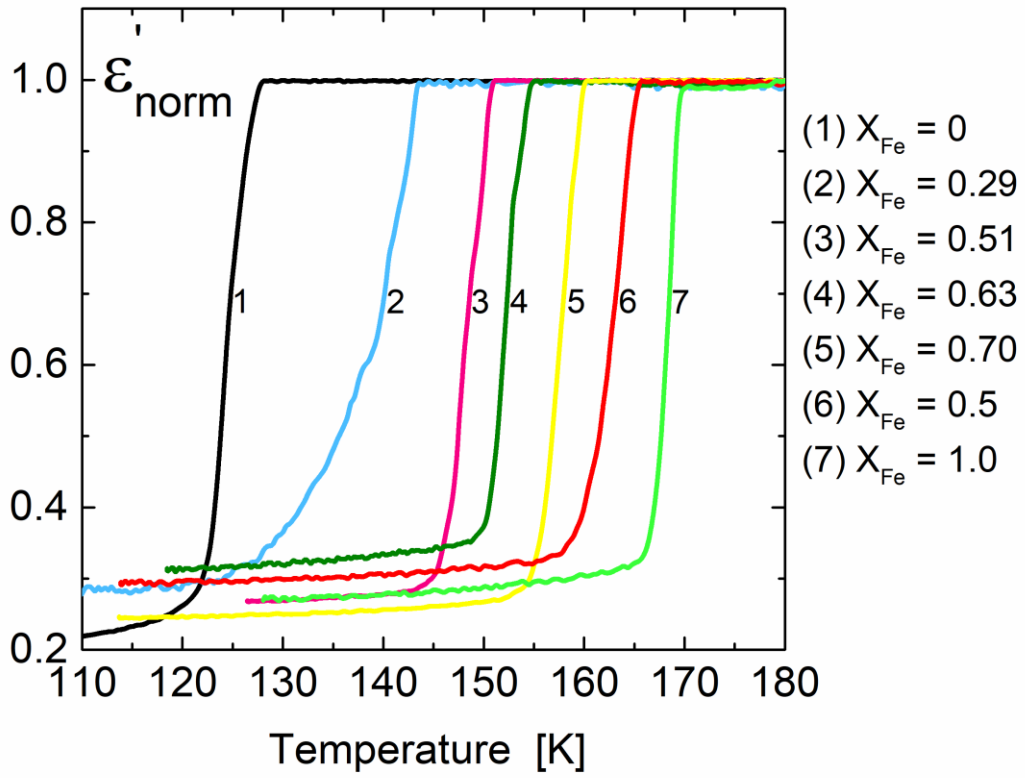

Fig. S7. Normalized dielectric response for pure **IMCFe** (x=1), **IMCo** (x=0) and for mixed-crystals **IMFe$_x$Co$_{1-x}$** (x = 0.29, 0.51, 0.63, 0.70 and 0.85).

a)

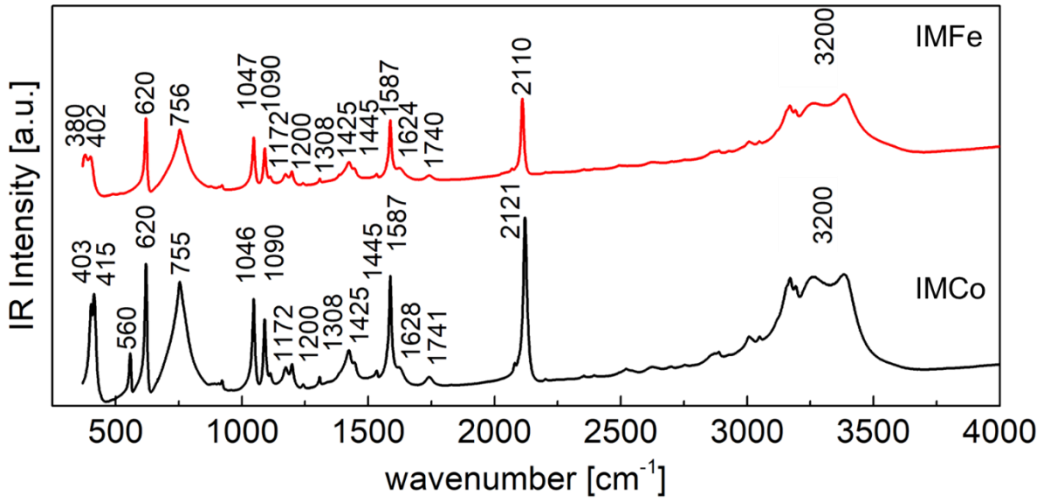

b) IMFe

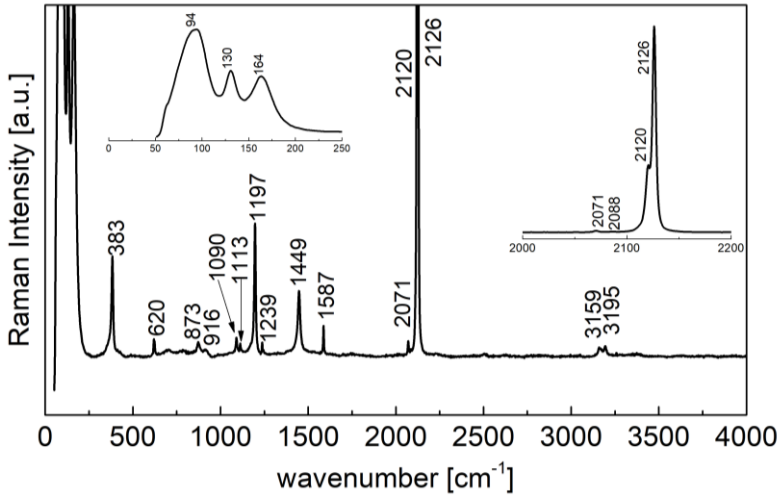

c) IMCo

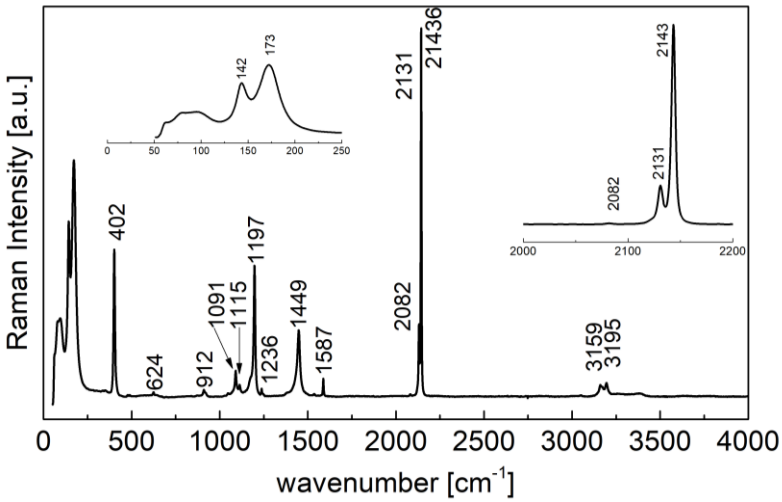

Fig. S8. a) IR spectra measured for pure **IMFe** and **IMCo** in KBr. Raman spectra for b) **IMCo** and c) **IMFe**.

Table S9. Observed IR and Raman frequencies (in cm^{-1}) and their assignments for (**IMFe**) and (**IMCo**) perovskites.

Approximate assignments	IMFe		IMCo	
	IR	Raman	IR	Raman
νN-H				
νN-H				
νC-H				
νC-H				
νC-H				
νC≡N (A_{1g})		2126		2143
νC≡N (E_g)		2120		2131
νC≡N (T_{1u})	2110		2110	
νC≡N (E_g)		2071 sh		2082 sh
νC=C , δN-H	1624		1628	
νC-N , δC-H	1587	1587	1587	1587
νC=C , νC-N , δN-C-N , δN-H	1445	1449	1445	1449
δN-H , νC-N	1425		1425	
δC-H	1308		1308	
νC-N	1200	1197	1200	1197
δC-H , νC-N , δN-H	1172		1172	
δC-H , νC-N	1090	1090	1090	1091
δN-H , νC-N	1047		1046	
δN-H , δRing, δC-H				
δRing		916		912
δRing		873		
$\rho_{w.}$C-H				
$\rho_{w.}$C-H				
$\rho_{w.}$C-H				
$\rho_{w.}$N-H	756		755	
$\rho_{w.}$N-H				
$\rho_{t.}$Ring		620		624
$\rho_{t.}$Ring	620		620	
Linear bending (Co-C≡N) (T_{1u})			560	
νFe/Co-C (A_{1g})		383		402
νFe/Co-C (T_{1u})	402		415	
νFe/Co-C (T_{1u})	380		403	
Angled bending (C-Fe/Co-C) (T_{2g}) , Linear bending (C-Fe/Co-C) (T_{2g})		164		173
Angled bending (C-Fe/Co-C) (T_{2g}) , Linear bending (C-Fe/Co-C) (T_{2g})		130		142
Angled bending (C-Fe/Co-C) (T_{2g}) , Linear bending (C-Fe/Co-C) (T_{2g})		94		80

ν-streching, δ-deformation (bending), $\rho_{t.}$-torsion, $\rho_{w.}$-wagging

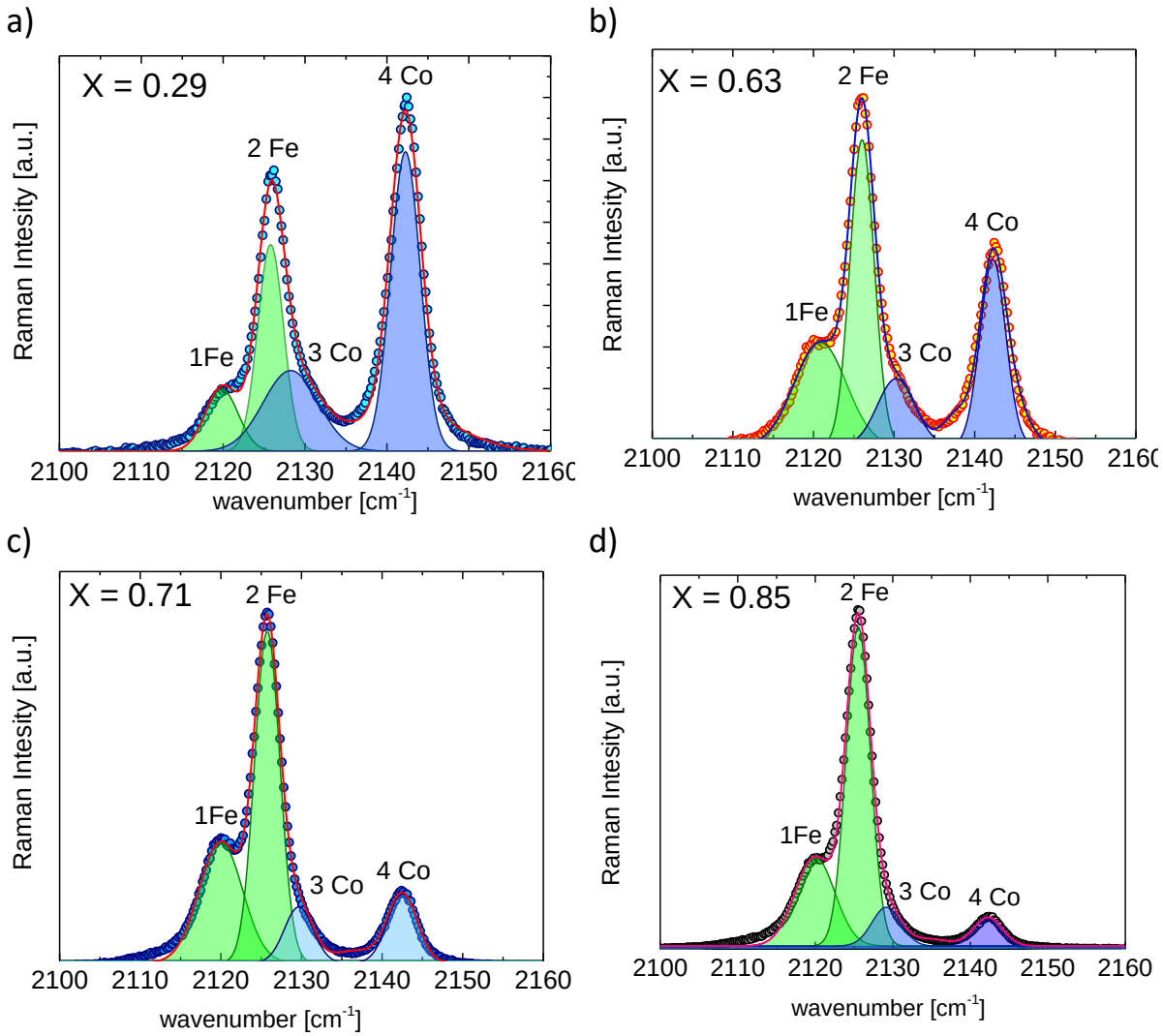

Fig. S9. Example of fitting of four peaks assigned to C≡N stretching modes in order to estimate stoichiometry of mixed crystals.

Table S10. Areas obtained all peaks marked in Fig. S7.

X Fe3+	No Peak / Area			
	1 Fe	**2 Fe**	**1 Co**	**2 Co**
0.29	0.1509	0.3953	0.3263	0.9540
0.63	0.3466	0.4760	0.1632	0.3084
0.71	0.3994	0.6408	0.2317	0.1954
0.85	0.4118	0.9072	0.1312	0.0964

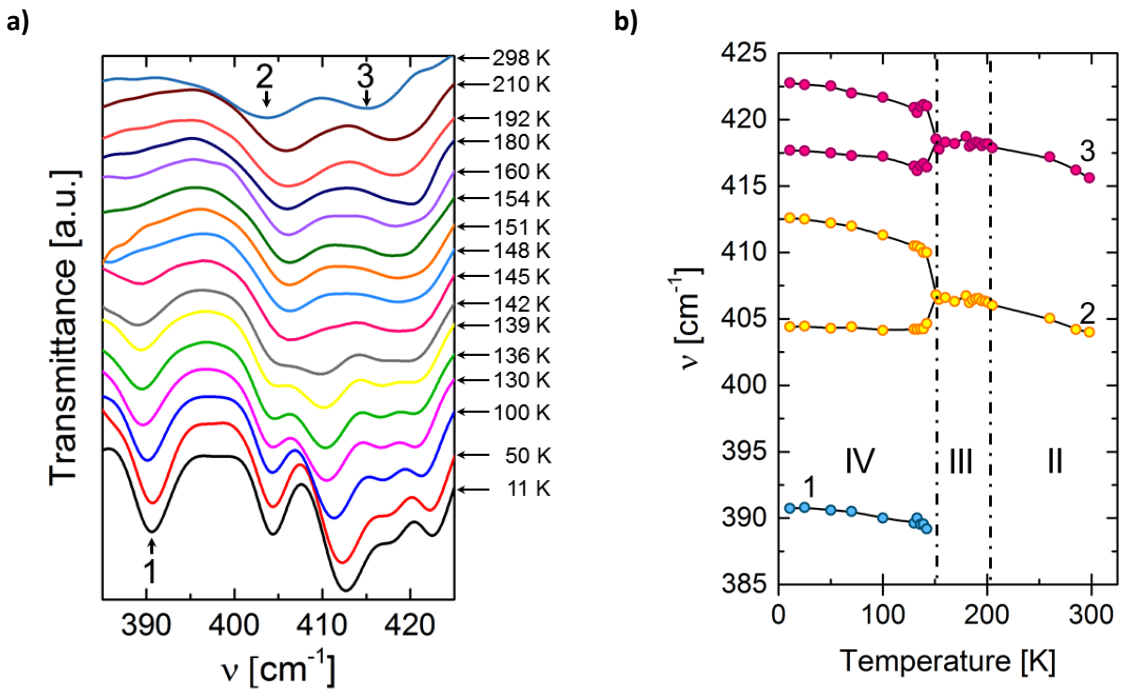

Fig. S10. a) Temperature evolution of bands assigned to Fe/Co-C stretching between 390 and 430 cm^{-1}; (b) temperature dependencies of the band positions.

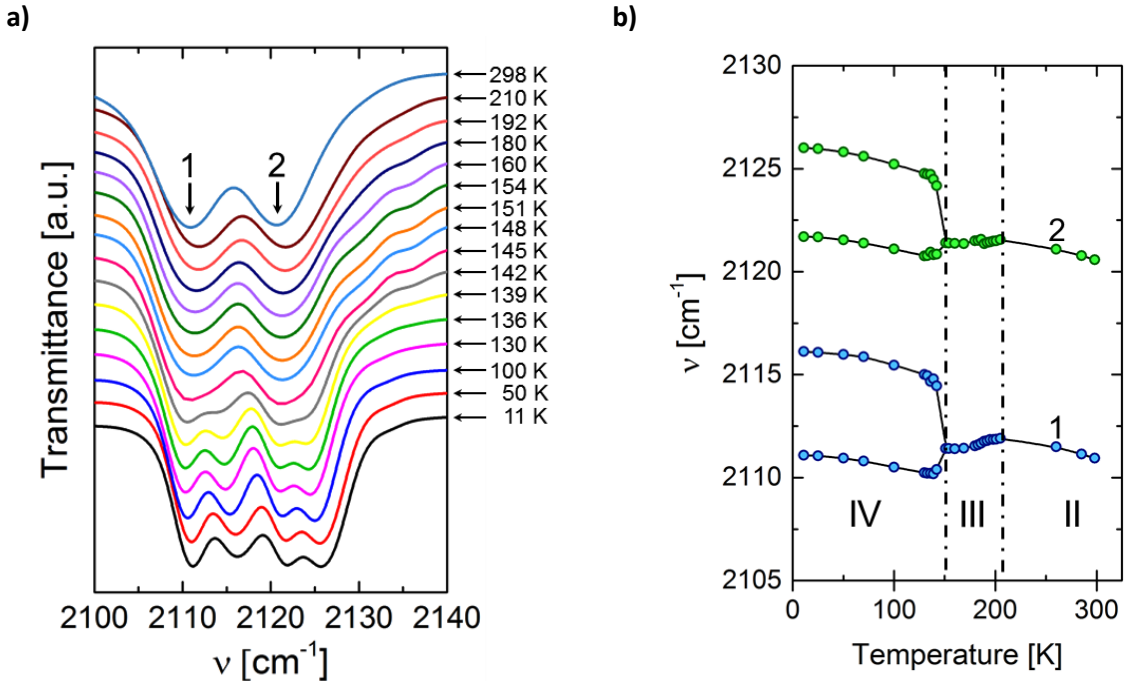

Fig. S11. a) Temperature evolution of bands assigned to C≡N stretching between 2100 and 2140 cm^{-1}; (b) temperature dependencies of the band positions.

a) b)

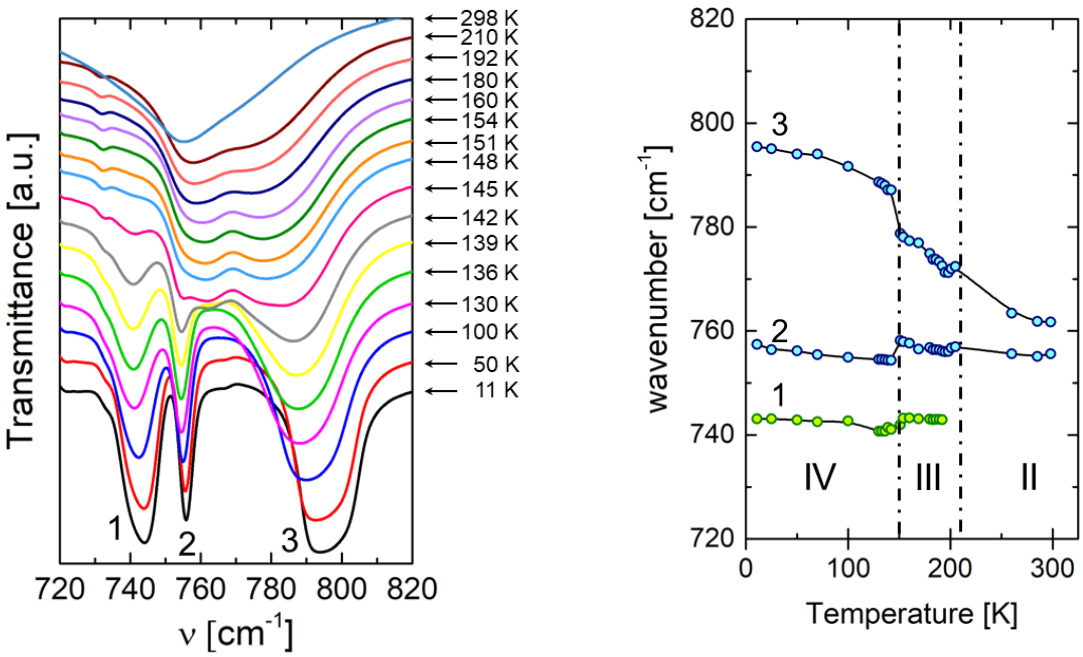

Fig. S12. a) Temperature evolution of bands assigned to out-of-plane hydrogen bond (N-H···N) vibration between 720 and 820 cm^{-1}; (b) temperature dependencies of the band positions.

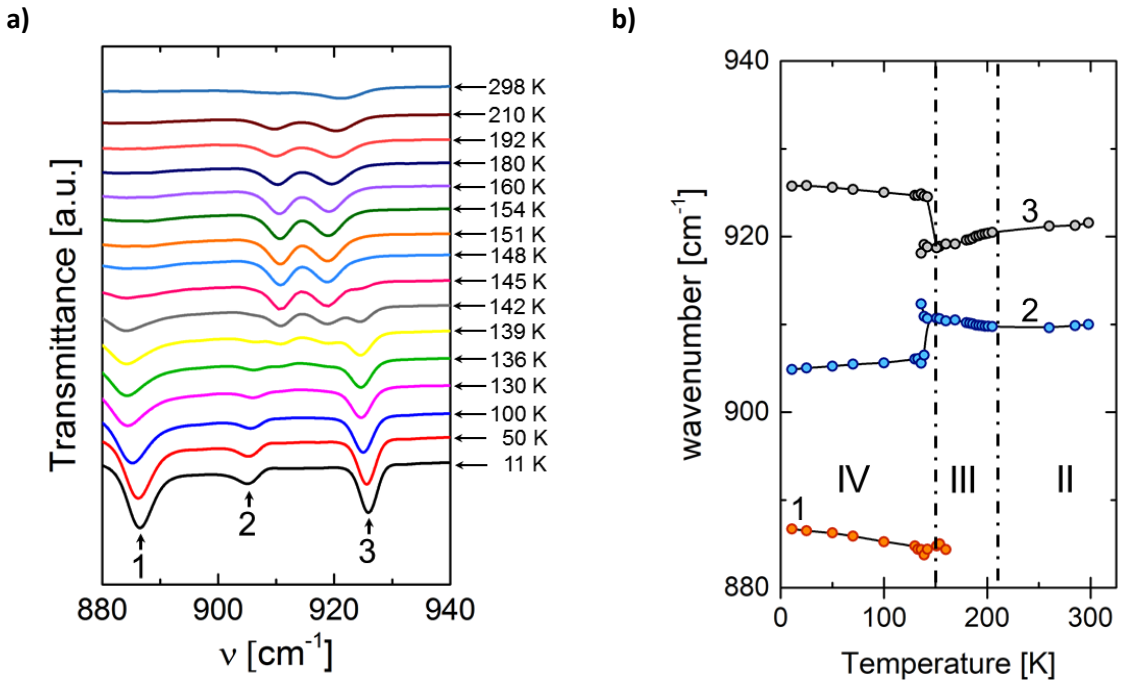

Fig. S13. a) Temperature evolution of bands assigned to imidazolium ring deformation between 880 and 940 cm^{-1}; (b) temperature dependencies of the band positions.

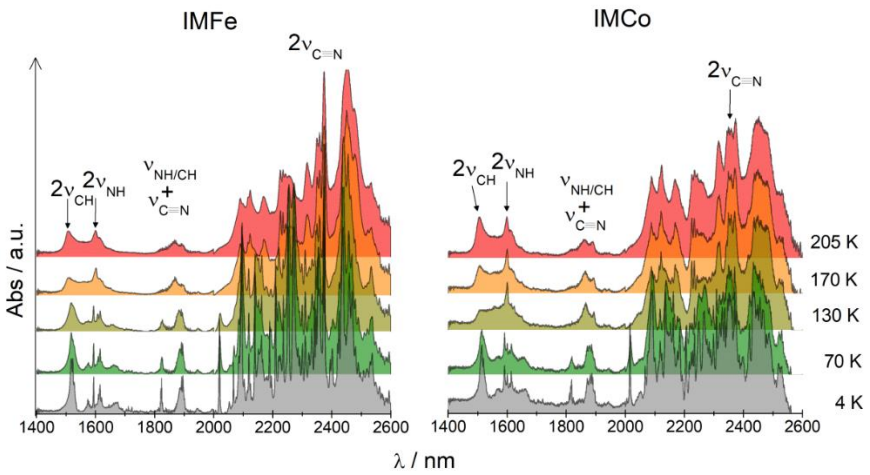

Fig. S14. NIR spectra versus temperature measured for pure **IMCo** and **IMFe** monocrystals